Res. Chem. Intermed., Vol. 34, No. 1, pp. 67–83 (2008)

Also available online - www.brill.nl/rci

Photocatalytic degradation of dimethyl phthalate ester using novel hydrophobic TiO_2 pillared montmorillonite photocatalyst

XUEJUN DING [1,2], TAICHENG AN [1,*], GUIYING LI [1], JIAXIN CHEN [1,2], GUOYING SHENG [1], JIAMO FU [1] and JINCAI ZHAO [3]

[1] *State Key Laboratory of Organic Geochemistry, Guangdong Key Laboratory of Environmental Resources Utilization and Protection, Guangzhou Institute of Geochemistry, Chinese Academy of Sciences, Guangzhou 510640, China*
[2] *Graduate School of Chinese Academy of Sciences, Beijing 100049, China*
[3] *Laboratory of Photochemistry, Center for Molecular Science, Institute of Chemistry, Chinese Academy of Sciences, Beijing 100080, China*

Received 15 July 2007; accepted 23 August 2007

Abstract—TiO_2 pillared montmorillonites were prepared by introducing Ti^{4+} into a layer of montmorillonite modified with or without cetyltrimethylammonium bromide. The components and texture of the prepared composites were characterized by thermogravimetric analysis, X-ray powder diffraction and scanning electron microscopy. The adsorption and photocatalytic degradation performance of a model environmental endocrine disruptor, dimethyl phthalate ester, were investigated using this newly prepared hydrophobic TiO_2 pillared montmorillonite photocatalyst. The adsorption of dimethyl phthalate ester from water varied from 9% to 28% on the prepared hydrophobic photocatalyst. Although the experimental results showed that the photocatalytic activity of the hydrophobic photocatalyst was slightly lower than that of hydrophilic one, electron spin resonance verified that hydroxyl radicals were also generated in hydrophobic TiO_2 pillared montmorillonite photocatalyst under UV irradiation. To elucidate the decomposition mechanism of dimethyl phthalate ester, 12 main photocatalytic intermediates were identified during the photocatalytic degradation process, and a plausible degradation mechanism was also proposed.

Keywords: Pillared clay; synthesis; dimethyl phthalate ester; adsorption; photocatalysis; degradation pathways.

*To whom correspondence should be addressed. Tel.: (86-20) 8529-1501; Fax: (86-20) 8529-0706; e-mail: antc99@gig.ac.cn

INTRODUCTION

Phthalate esters (PAEs) are widely used in chemical industries across the world. Several million tons are produced annually and about 85% of the amount produced is used as plasticizers for polyvinyl chloride (PVC) resins, adhesives and cellulose film coating [1, 2]. Additionally, PAEs are used as a component of solvents, repellents, flotation reagents, and in the production of cosmetics, lubricants, textiles and other products [3, 4]. Dimethyl phthalate ester (DMP), a short-chained ester among PAEs, is widespread in the environment because of its common usage and its refractory biodegradability. It has been detected in many natural environments such as fresh waters, marine waters, soil and sediments [5]. Moreover, DMP can be bioconcentrated and biomagnified in the aquatic food chain [6]. Potential sources of DMP are mainly thought to be through the release of wastewater from production and processing activities, and the release from usage and disposal of materials containing phthalate esters [2, 7]. However, the long-term exposure to DMP can cause functional disturbances in the nervous system and liver of animals. It is also suspected to have endocrine-disrupting activity, and result in decreased fertility in human beings and other organisms [8]. Thus, because of its ecological toxicity and hazard, DMP has been designated as a Priority organic pollutant by the United States Environmental Protection Agency (US EPA) and other European countries [9].

Due to the low solubility in water and low biodegradability of DMP, some proper technologies need to be developed to remediate the pollution of DMP. Some recent treatment technologies are mainly focused on the biodegradation under both aerated and anoxic conditions by various microorganisms [10–12]. The advanced oxidation processes, employing the TiO_2 or Fenton reagent as photocatalyst under UV or sunlight irradiation [13–16], have also been reported frequently as alternative treatment methods. However, the concentration of DMP in ambient waters is quite low and the adsorption of DMP onto a commercial TiO_2 photocatalyst is very limited because of the latter's hydrophilic properties and small specific surface area. Thus, the photocatalytic degradation rate is often very low in much diluted environmental conditions such as occur in natural waters. Hence, the enrichment of organic pollutants onto the catalysts may be a prerequisite to achieve high photocatalytic degradation efficiency.

Recently, pillared clays have attracted much attention as a new kind of porous materials. This composite material is prepared by intercalating organic or inorganic cations into the silicate layers of clays to form diversified pillared materials after treatment. The cation surfactants pillared clays possess much larger specific surface area than original clay because of the existence of micropores and mesopores. This and the increased hydrophobicity make them an excellent adsorbent for organic pollutants in water [17–20]; on the other hand, some inorganic pillared clays, such as TiO_2 and CdS pillared clays, show good photocatalytic activity for organic pollutants in water [21–24]. However, adsorption is the first step for the photocatalytic degradation of organic pollutants. But, as far as pillared

clay is concerned, the clay and TiO_2 are all hydrophilic, while most of the persistent organic pollutants in the environment are hydrophobic. As a result, the photocatalytic reaction rate decreases significantly if the adsorption of persistent organic pollutants onto the TiO_2 pillared clay is very limited. Thus, increasing the adsorption of organic pollutants onto photocatalysts may enhance the degradation rate of organic pollutants because the photocatalytic degradations are the surface reaction.

In this paper, a novel hydrophobic TiO_2 pillared clay photcatalyst was prepared by sol–gel method at certain ratio of $Ti(OC_4H_9)_4$ to HCl modified by different kinds of surfactants, such as cetyltrimethylammoniumbromide (CTMAB). This original work focus on the combination of the pre-adsorption and concentrated effect for micro-pollutants on newly synthesized hydrophobic TiO_2 pillared montmorillonites with the photocatalytic destruction for organic pollutants on nanometer titanium dioxides pillared in montmorillonite. DMP was used as model organic pollutant to investigate adsorption and photocatalytic activity of prepared photocatalyst. The results showed that the adsorption capacity of prepared material has been increased greatly with treated with CTMAB. These conclusions will play an important role in better understanding of the transfer, transform and photochemical degradation of organic pollutants, such as PAEs, in the geochemistry recycle.

EXPERIMENTAL

Materials and apparatus

The raw montmorillonite clay was obtained from Lin'an (Zhejiang, China). Its major chemical composition is: 57.13% SiO_2; 0.18% TiO_2; 17.31% Al_2O_3; 1.65% Fe_2O_3; 0.03% MnO; 3.11% MgO; 1.78% CaO; 2.32% Na_2O; 0.38% K_2O. The clay powder has a specific surface area of 18.03 m^2/g and a cation exchange capacity (CEC) of 54.47 mmol/100 g. Titanium tetraisoproproxide was used without further purification to prepare the sol of titanium hydrate. The reaction substrate, DMP, was an analytical grade reagent, and the spin trap 5,5-dimethyl-1-pyrroline-*N*-oxide (DMPO) was purchased from Sigma (St. Louis, MO, USA), while the derivative reagents, *N*,*O*-bis (trimethysilyl)-trifluoroacetamide (BSTFA) was purchased from Arcos. Methylene chloride was re-distilled using a glass system, and other chemicals, such as CTMAB, were all analytical grade reagents, and all aqueous experiments were carried out in deionized water. Thermogravimetric analysis (TGA) of prepared pillared clays was measured on a Netzsch TG209 thermogravimetric analyzer. About 6 mg of sample was heated from ambient temperature to 1103 K at a heating rate of 10.0 K/min in the atmosphere of air. A Rigaku D/Max 2200 VPC powder diffractometer with Cu Kα radiation (λ = 0.15418 nm), the accelerating voltage of 40 kV, emission current of 30 mA and the scanning speed of 10°C/min was used to determine the crystal phase composition of the prepared materials at room temperature. A scanning electron microscope (SEM,

LEO 1530 VP) was used to observe the microstructure and size of the prepared photocatalysts.

Synthesis of pillared clays

The montmorillonite clay was modified with CTMAB by a cation-exchange process using a 2:1 molar ratio of CTMAB to CEC after it was swollen in water (1 g/100 ml) for 24 h. The mixture was stirred continuously for 48 h and washed with deionized water for several times. The titanium hydrate sol (prepared by sol–gel method with titanium tetraisoproproxide added to hydrochloric acid solution, aged for 4 h) was added slowly drop-wise into the solution of washed clay with different molar ratios of Ti/CEC (20:1, 40:1, 60:1) and then stirred for another 48 h. The suspension was then centrifuged and washed with deionized water again, and the resulting wet cakes were dried thoroughly at 333 K, calcinated at different temperatures, and then ground into powder to obtain and named as hydrophobic TiO_2 pillared clay. The TiO_2 pillared clay without a surfactant modifier was also synthesized in a comparable fashion except no CTMAB was added in this case.

Adsorption and photocatalytic degradation of DMP

The adsorption and photocatalytic degradation of DMP were carried out in a quartz tube (150 ml) with a double-walled cooling-water jacket to keep the temperature of solutions constant throughout all experiments. The light source, which was a high-pressure mercury lamp (GGZ-125, Shanghai Yaming Lighting, $E_{max} = 365$ nm) with a power consumption of 125 W, was housed in one side of the photoreactor to provide the irradiation. Prior to illumination, a suspension of 150 ml DMP (50 mg/l) including 0.3 g photocatalyst was stirred in the dark for 30 min to achieve the adsorption equilibrium. Then the UV light was turned on for the photocatalytic degradation experiments. 5 ml DMP solution was sampled at fixed intervals, filtered and used for DMP analysis.

Analysis

5 ml sampled DMP solution was extracted with 3 ml re-distilled CH_2Cl_2 three times. All extracted solvent phases were collected and mixed, then dried with Na_2SO_4 and the volume adjusted with CH_2Cl_2 to 10 ml. The DMP concentration was determined with HP 6890 Series GC system equipped with a HP-5 capillary column (30 m × 0.32 mm i.d., film thickness 0.25 μm). Column temperature was held at 80°C for 10 min and then heated to 300°C at a rate of 35°C/min. Injector and detector (FID) temperatures were 260°C and 300°C, respectively; nitrogen was used as carrier gas with a velocity of 1.5 ml/min. To determine the intermediates arising from degradation, the fixed 10 ml samples were blown to dryness under a gentle N_2 stream, and then these samples were injected into the GC-MS for the qualitative analysis after the dried extracts were silylated by addition of 50 μl of pyridine and

50 µl of BSTFA in a sealed vial overnight. For GC/MS analysis, a HP 6890GC with a Micromass Platform II mass selective detector (MSD) operated in the scan mode was used to identify the intermediates. The GC column employed was a HP-5 fused-silica capillary column and the initial oven temperature was held at 80°C for 8 min, and then heated to 295°C at a rate of 10°C/min with helium as a carrier gas.

RESULTS AND DISCUSSION

Characterization of prepared TiO_2 pillared clay photocayalysts

Thermogravimetric analysis. The thermogravimetric analysis (TGA) profiles of raw montmorillonite clay, TiO_2 pillared clay and hydrophobic TiO_2 pillared clay are shown in Fig. 1. It can be seen from Fig. 1 that the raw clay and TiO_2 pillared clay have similar weight loss curves. These two clays lost about 15% and 10%, respectively, of their weight within 453 K, indicating the dehydration of adsorbed water [25]. The raw clay has another 5% weight loss beyond 873 K due to the large range of collapse of interlayer and mesopores of montmorillonite [26]. This weight loss cannot be found in the TGA curve of TiO_2 pillared clay, which suggests the formation of TiO_2 pillars between interlayers, keeping the structure well under same high calcination temperature. In contrast, hydrophobic TiO_2 pillared clay has no great weight loss below 473 K because the exchanged organic anion surfactant pillared inside of the clay leads to the pillared clay becoming too hydrophobic. This result is similar to another report stating that the pillared clay exchanged

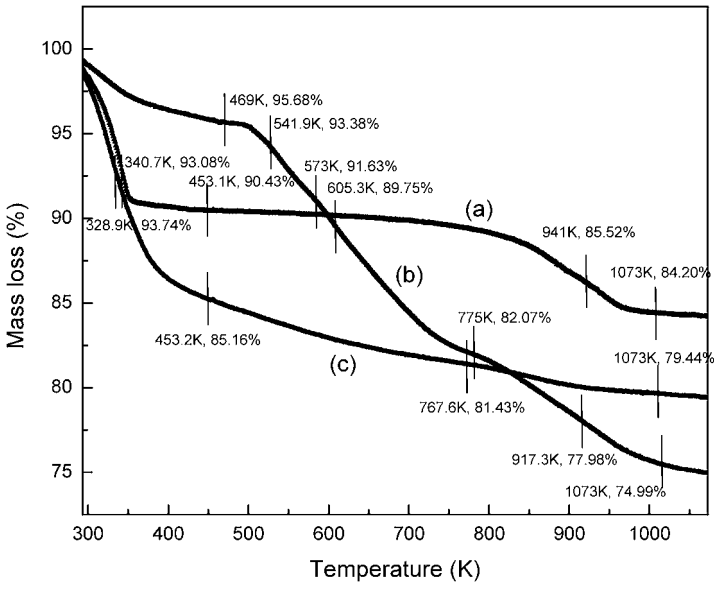

Figure 1. TGA pattern of different clays: (a) Montmorillonite; (b) Hydrophobic TiO_2 pillared clay; (c) TiO_2 pillared clay.

with organic surfactant has good surface hydrophobicity and contains much lower contents of water [27]. It can be assumed that the hydrophobic TiO_2 pillared clay is more hydrophobic than raw clay and TiO_2 pillared clay, which indicates that the hydrophobic TiO_2 pillared clay would possess better adsorption capability for hydrophobic organic pollutants from the water. However, the hydrophobic TiO_2 pillared clay has 13% mass loss in the temperature range from 473 K to 773 K and another 13% weight loss beyond 773 K. The former drop is mainly attributed to the combustion of CTMAB inside the clay layer, while the latter is mainly due to the collapse of interlayer space of pillared clay. This can be interpreted as follows: The excess Ti^{4+} (originated from Ti-sol) exchanges a portion of CTMAB from clay and leads to some TiO_2 deposited onto the surface of the organic pillared clay rather than in the interlayer of clay. Thus, this partially organic exchanged TiO_2 pillared clay has a lower thermal stability than TiO_2 pillared clay when calcined at temperatures higher than 773 K, suggesting that the hydrophobic TiO_2 pillared clay can be synthesized under properly controlled calcination temperature.

X-ray diffraction (XRD) patterns. Figure 2 shows the XRD patterns in the small-angle range of the raw montmorillonite clay, TiO_2 pillared clay and hydrophobic TiO_2 pillared clay. As shown in this figure, the raw clay displays the (001) diffraction peak at $2\theta = 6.8°$, indicating that the basal spacing is 1.3 nm, and this peak is not observed in the XRD patterns of the other two pillared clays. This result is in accordance with a previously published reference that the pillared clay does not have a sufficiently ordered and oriented silicate layer structure to show the

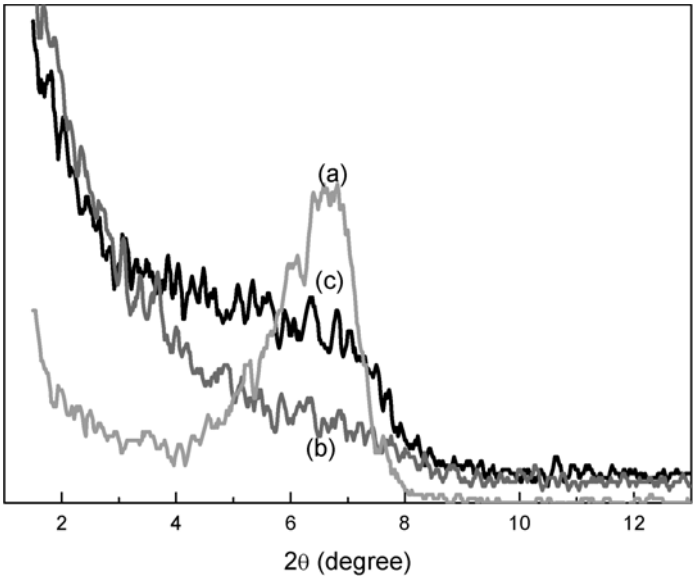

Figure 2. XRD patterns in small angle of different clays: (a) Montmorillonite; (b) TiO_2 pillared clay, $T = 673$ K; (c) Hydrophobic TiO_2 pillared clay, $T = 673$ K.

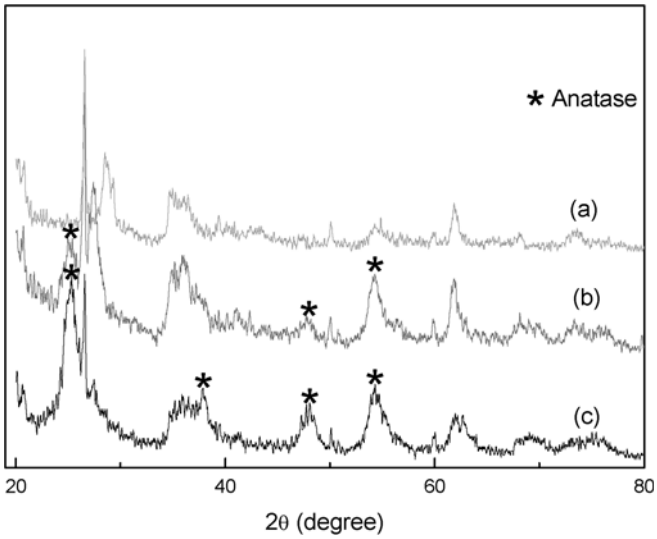

Figure 3. XRD patterns in wide angle of different clays: (a) Montmorillonite; (b) TiO_2 pillared clay, $T = 673$ K; (c) Hydrophobic TiO_2 pillared clay, $T = 673$ K.

(001) peak [24]. The wide-angle XRD patterns also have been shown in Fig. 3. There are only few typical adsorption peaks of montmorillonite in the raw clay [28]. However, the typical peaks due to anatase phase TiO_2 appear in the XRD patterns of hydrophobic TiO_2 pillared clay and TiO_2 pillared clay. The average size of the anatase TiO_2 particles in both pillared clay samples were calculated with X-ray diffraction peak at $2\theta = 25.3^\circ$ (101) using the Debye–Scherrer equation [29]. The average sizes of the anatase TiO_2 in hydrophobic TiO_2 pillared clay and TiO_2 pillared clay were calculated as 19.9 nm and 14.2 nm, respectively.

Figure 4 also shows the XRD patters of the hydrophobic TiO_2 pillared clays calcinated at different temperatures. It can be seen that these pillared clays have almost the same patterns, the typical anatase TiO_2 peaks can be observed in the XRD curves. However, the typical anatase TiO_2 peak $2\theta = 25.3^\circ$ increased dramatically with the increment of calcination temperatures. The average sizes of anatase TiO_2 were calculated as 17.2 nm, 19.9 nm, 22.7 nm and 25.3 nm at 573 K, 673 K, 773 K and 873 K, respectively. It is easily seen that the average size of anatase particles becomes larger and larger with the increment of calcination temperatures.

Scanning electron microscopy (SEM). The SEM images of raw montmorillonite, hydrophobic TiO_2 pillared clay and TiO_2 pillared clay are shown in Fig. 5. It can be clearly seen that the original structure of clay is maintained much better in TiO_2 pillared clay when pretreated with CTMAB. It can be seen from Fig. 5a and 5b that both the raw montmorillonite and hydrophobic TiO_2 pillared clay exhibit good microporous and interlayer structure, while in Fig. 5c the interlayer structure of clay is damaged. After the clay is pillared with inorganic cations, it does not have a sufficiently ordered and oriented silicate layer [24]. This suggests that the presence

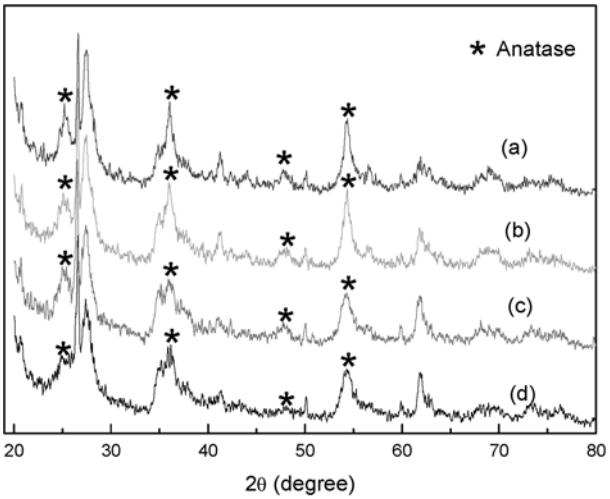

Figure 4. XRD patterns in wide angle of hydrophobic TiO_2 pillared clays calcinated at different temperatures: (a) $T = 873$ K; (b) $T = 773$ K; (c) $T = 673$ K; (d) $T = 573$ K.

Figure 5. SEM photographs of different clays: (a) montmorillonite; (b) hydrophobic TiO_2 pillared clay, $T = 673$ K; (c) TiO_2 pillared clay, $T = 673$ K.

of cation surfactants helps to keep the original structure of the clay when titanium ions are exchanged into the interlayers of clay.

Adsorption and photocatalytic degradation of DMP

It is well known that the adsorption of organic pollutants from aqueous solutions onto clay is not only influenced significantly by the specific surface area, but also affected by the hydrophobicity or the polarity of adsorbents. Na^+ and Ca^{2+} pillared montmorillonites or TiO_2 pillared montmorillonite are all classified as hydrophilic materials. However, when the clay is modified with surfactants its surface will generally become more hydrophobic. In order to investigate this effect, the adsorption profile of hydrophobic TiO_2 pillared clay was compared with unmodified TiO_2 pillared clay and the result is shown in Fig. 6. From Fig. 6, we can

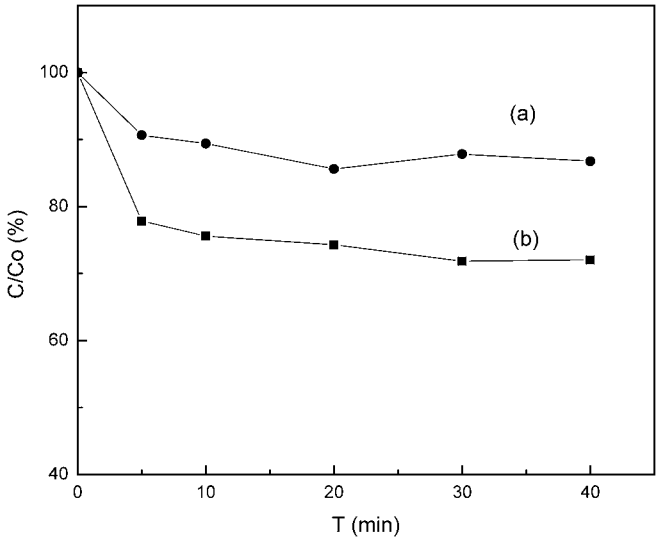

Figure 6. The removal efficiencies of DMP by adsorption on hydrophobic TiO_2 pillared clay and TiO_2 pillared clay: (a) TiO_2 pillared clay, $T = 673$ K; (b) Hydrophobic TiO_2 pillared clay, $T = 673$ K.

clearly see that only 13% of DMP was adsorbed by TiO_2 pillared clay, as compared to 28% adsorption of DMP on the hydrophobic TiO_2 pillared clay. This is due to the increased hydrophobicity of organic modified TiO_2 pillared clay. However, in the TiO_2 pillared clay, the surface remains hydrophilic after exchange with titanium ions. Thus this may be the reason why there are differences in the adsorption efficiency of DMP between TiO_2 pillared clay and hydrophobic TiO_2 pillared clay.

The adsorption performance of hydrophobic TiO_2 pillared clays calcined at different temperatures is also presented in Fig. 7. It can be seen from this figure that hydrophobic TiO_2 pillared clay samples calcined from 573 K to 873 K have similar adsorption trends for DMP. The adsorption rates of DMP increased rapidly within first 5 min, and equilibrium was achieved within 20 min in all tests. And the adsorption efficiency of DMP decreased slightly with the increase in the calcination temperatures. This is probably due to the decomposition of existing organic matter existed in pillared clay during calcination from 573 K to 873 K according to thermogravimetric analysis data reported above in this paper. Thus, the surface hydrophobicity of calcinated pillared clay was lost when the calcination temperature becomes too high.

All photochemical and photocatalytic degradation were conducted under same conditions after adsorption equilibriums have been achieved. As shown in Fig. 8, the photolysis efficiency of DMP is very slow (22% in 60 min). The photocatalytic activity of two prepared pillared clay modified with and without surfactants were compared, and the degradation curves were also shown in Fig. 8. The TiO_2 pillared clay has slightly higher activity than the hydrophobic TiO_2 pillared clays, even though its adsorption capability of DMP is lower than the latter. It can be explained

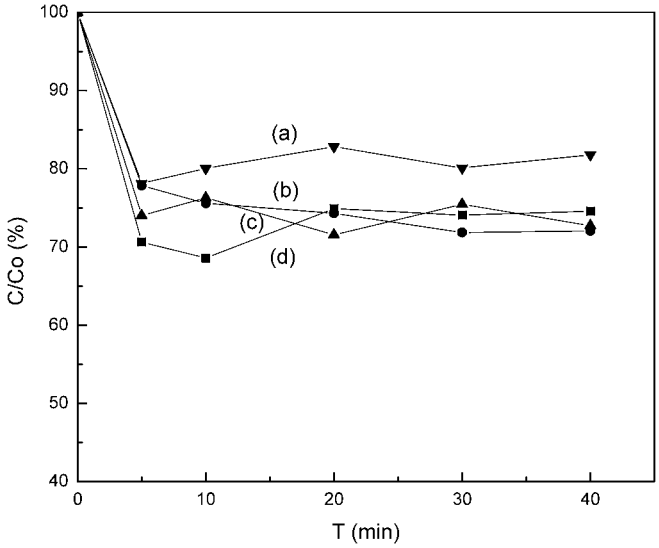

Figure 7. The removal efficiencies of DMP by adsorption on hydrophobic TiO_2 pillared clays calcinated at different temperatures: (a) $T = 873$ K; (b) $T = 673$ K; (c) $T = 773$ K; (d) $T = 573$ K.

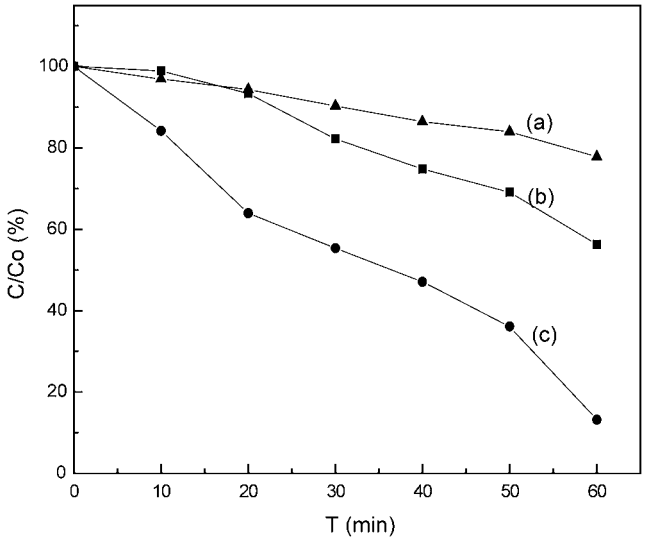

Figure 8. Degradation kinetics of DMP by hydrophobic TiO_2 pillared clay and TiO_2 pillared clay: (a) Photolysis of DMP; (b) Hydrophobic TiO_2 pillared clay, $T = 673$ K; (c) TiO_2 pillared clay, $T = 673$ K.

by the carbon deposits originated from the combustion of CTMAB when the cation surfactant pillared clay calcined at high temperature. These carbon deposits on the pillared clay may slightly block the irradiation of UV light to TiO_2. Moreover, the XRD patterns also shown that the hydrophobic TiO_2 pillared clays have poorer crystallized anatase phase than TiO_2 pillared clays. Although the hydrophobic

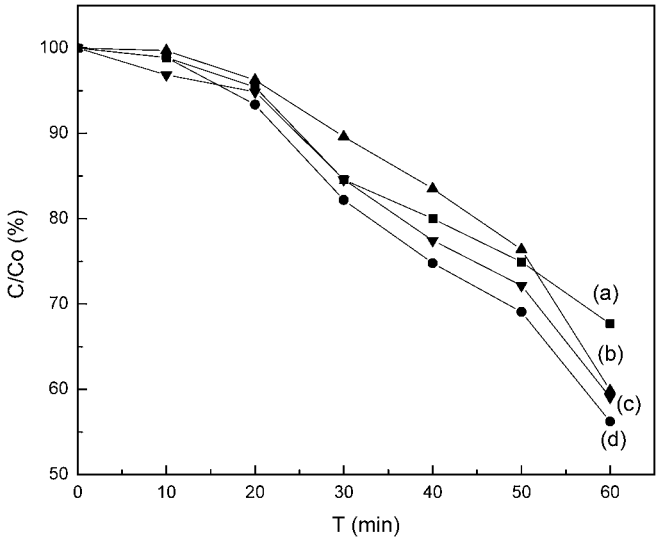

Figure 9. Degradation kinetics of DMP by hydrophobic TiO_2 pillared clays calcinated at different temperatures: (a) $T = 573$ K; (b) $T = 773$ K; (c) $T = 873$ K; (d) $T = 673$ K.

TiO_2 pillared montmorillonite has lower photocatalytic activity than TiO_2 pillared montmorillonite, the authors think this may be play an important role in better understanding of the transfer, transform and photochemical degradation of PAEs onto some natural geoadsorbents in the geochemistry cycle.

The effect of calcination temperature on the photocatalytic acivity of hydrophobic TiO_2 pillared clay is shown in Fig. 9. The degradation rate of DMP increases with the increase in calcination temperature up to a maximum at 673 K, and then decreases slightly after this temperature. The high photocatalytic activity of TiO_2 pillared clay was obtained at lower calcination temperature, which is attributed to quantum size effects. However, the photocatalytic activity of TiO_2 pillared clay calcined at 573 K is slightly lower than that of the photocatalyst calcined at 673 K, which may be due to the partial formation of crystallite oxides. With further increase in the calcination temperature, the average size of titanium dioxide also increases, which is supported by XRD spectrum, resulting in a reduction in quantum size effects. At same time, when temperature is higher than 873 K, anatase TiO_2 particles pillared in clay partly transform to the rutile phase which is a poor photocatalyst, resulting in a significant reduction in the photocatalytic activity of hydrophobic TiO_2 pillared clay.

Evidence for the presence of $^{\bullet}OH$ radicals

It is well known that the photocatalytic degradation process of organic pollutants proceeds *via* the oxidation by photogenerated holes and its resultant $^{\bullet}OH$ under UV

irradiation and the reaction mechanisms are demonstrated as below:

$$TiO_2 \xrightarrow{h\nu} e^- + h^+, \quad (1)$$

$$h^+ + H_2O \longrightarrow {}^\bullet OH + H^+, \quad (2)$$

$$e^- + O_2 \longrightarrow O_2^-. \quad (3)$$

In the present paper, in order to verify the generation of $^\bullet$OH radical in the photocatalytic process using prepared hydrophobic TiO_2 pillared montmorillonite as photocatalysts, ESR spectroscopy using spin traps was employed to investigate the existence of the hydroxyl radicals. The ESR spectrum of DMPO spin trap adduct is shown in Fig. 10. The characteristic ESR signal of DMPO-$^\bullet$OH adduct with the four fold peaks having an intensity ratio of 1:2:2:1 [30] was observed, which indicated that the hydroxyl radicals are indeed generated under UV irradiation of the hydrophobic TiO_2 pillared clays. Thus, we can conclude that the degradation mechanisms of organics by prepared hydrophobic TiO_2 pillared clays involve the generation and reaction with $^\bullet$OH as in other photocatalytic processes to some degree [31, 32]. The dependence of the peaks intensity on irradiation time is also presented in Fig. 10. From Fig. 10, we can see that there are no signals in the absence of UV light (the base line), while the DMPO-$^\bullet$OH peaks appear instantly when UV light is turned on. Moreover, the intensity of adduct peaks increases

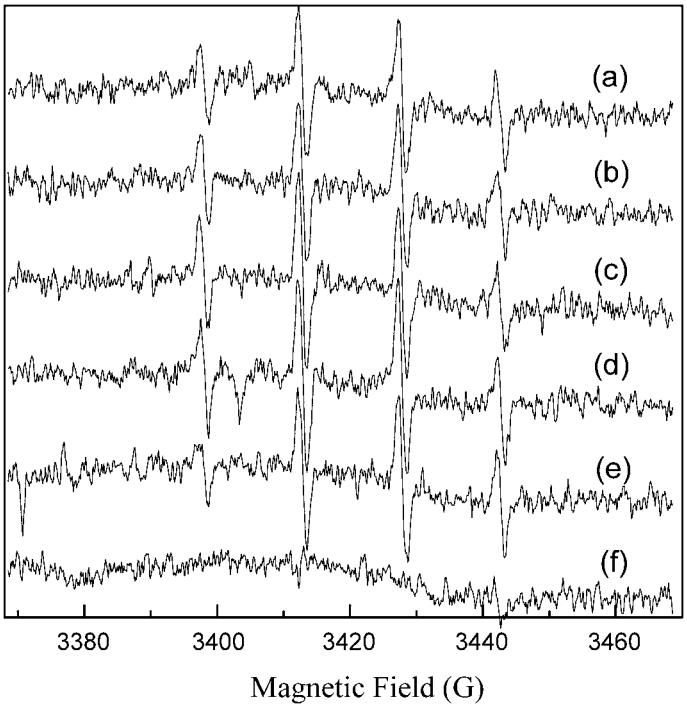

Figure 10. ESR signals of DMPO-$^\bullet$OH peaks at different irradiation time: (a) 323.78 s; (b) 242.872 s; (c) 161.961 s; (d) 81.135 s; (e) 0 s; (f) baseline.

slightly at first, and then drops gradually upon UV light irradiation of the aqueous solution.

Reaction mechanism and degradation pathways of DMP

A variety of degradation technologies have been examined to remove phthalate esters from water because of the refractory biodegradation and toxicity to organisms. Among these technologies, the photocatalytic degradation is promising in that it can achieve complete mineralization of the pollutants into less toxic or harmless compounds.

In the photocatalytic degradation of phthalate esters, there are two possible sites for the attack of •OH radicals, the alkyl chain and the aromatic ring, respectively. The reaction mechanisms can be summarized as follows, according to earlier studies [33–38]: the attack of hydroxyl radicals leads to the formation of hydroxyl or dihydroxyl photoproducts on aromatic ring for phthalates with shorter alkyl chains, while the attack of •OH radicals is dominant on the alkyl chain when the alkyl chain is longer than three carbon atoms. Thus, there are four possible pathways in the degradation of different dialkyl phthalates: (1) the attack of hydroxyl radicals on the aromatic ring; (2) the attack of hydroxyl radicals on alkyl chain; (3) the cleavage of the C–C bond connecting a carbonyl group with the aromatic ring; and (4) the scission of an ester group, leaving the dicarbonic acid structure intact. Pathways (1) and (2) are the dominant reaction during photocatalytic reaction, and pathways (3) and (4) take place in photolytic degradation of DMP. However, in all previously published studies on the photocatalytic degradation of phthalate esters, no intermediates arising from ring cleavage have been detected [33–38]. All the reaction mechanisms published to date have focused on the primary attack site and reaction routes but leave the aromatic ring intact. Therefore, much attention is paid to ring cleavage photoproducts in this paper.

The preferential reaction mechanism would be the attack of •OH radicals on the aromatic ring when DMP was used as model organic pollutant in this paper. A total of twelve products was identified by comparison of the mass spectrometry after derivatization with BSTFA and their molecular structures are all presented in Table 1. In first pathway, the aromatic ring must undergo addition of •OH radicals. In addition to product 1, we have unequivocally identified three dihydroxyl-methyl benzoates (products 3, 4 and 5). These three products were also reported during the degradation of DMP in the early references [34, 35]. These products can be formed by attack of another hydroxyl radical on different positions in the benzene ring and removal of an ester group from product 1 at the same position. These three products can also be formed by the double attack of •OH radicals on the benzene ring of product 2. It also known that the C–C bonds between the adjacent hydroxyl groups are readily oxidized. Thus, after further oxidation, these three intermediates give rise to another three ring cleavage intermediates, products 9, 10 and 11. These three advanced oxidation products have not been reported previously in the photocatalytic degradation of phthalate esters. Of course, these above-mentioned

Table 1.
Products of the degradation of DMP

GC/MS		
1	Hydroxylated DMP	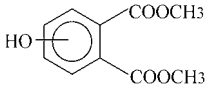
2	Methyl benzoate	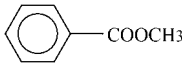
3	2,3-dihydroxy-methyl benzoate	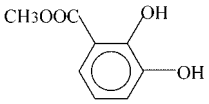
4	2,4-dihydroxy-methyl benzoate	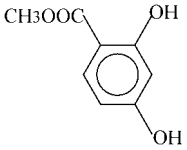
5	2,6-dihydroxy-methyl benzoate	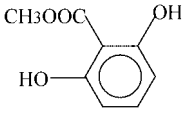
6	Benzoic acid	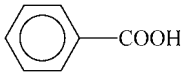
7	2,3-dimethyl-benzoic acid	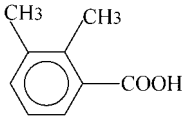
8	2-hydroxy-benzoic acid	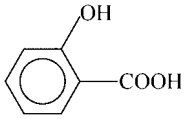
9	2,3-butanediol	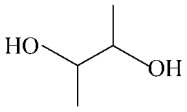
10	1,2-propanediol	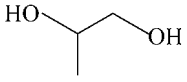
11	1,2-glycol	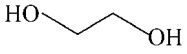
12	2-hydroxy-3-methyl-butyric acid	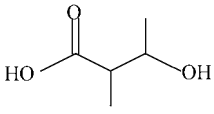

three intermediates would be mineralized into CO_2 and H_2O eventually. As far as the second pathway is concerned, because the alkyl chain in DMP is very short, the attack of hydroxyl radicals on the alkyl chain proceeds very difficultly and, hence, the dealkylation products, have not been observed in our experiments. Thus, we

can conclude that the second pathway is not dominant in our work. In the third pathway, a carbonyl group of DMP was excited after the adsorption of a photon and then led to the cleavage of one C–C bond connecting the $COOCH_3$ group to the aromatic ring. The resultant product 2 is detected in our reaction procedure. The product 2 undergoes a further single β-cleavage of the ester group, giving rise to product 6 and the sequentially removal of a $^{\bullet}CH_3$ radical leaving the dicarbonic acid (COOH) structure intact. The benzene ring of product 6 can be attacked by $^{\bullet}CH_3$ or $^{\bullet}OH$ radicals alternatively to generate products 7 and 8, respectively. The resulting intermediate product 7 can also be further decomposed completely into CO_2 and H_2O, while product 8 is followed by a ring-cleaving process to give rise to product 12, which also can be oxidized into CO_2 and H_2O at last. However, as for fourth pathway, we were unable to identify any primary intermediates obtained from the scission of ester group from DMP as should occur in the fourth pathway cited earlier. We believe, therefore, that the first and the third routes should be the dominant processes in the photocatalytic and photolytic degradation of DMP. A tentative degradation mechanism is proposed in Fig. 11.

CONCLUSIONS

The calcination temperatures have a great influence on the photoactivity and the adsorption capacity of prepared hydrophobic pillared clay. The adsorption efficiency of DMP decreased slightly with the increase of the calcination temperatures, while the degradation rate of DMP is increased with the increment of calcination temperature from 573 K, but exhibited a maximum at 673 K, and then decreased slightly after this temperature.

The ESR experiments showed that the hydroxyl radicals were indeed generated under UV irradiation when the hydrophobic TiO_2 pillared clays was used as a photocatalyst. Thus, the degradation mechanisms of DMP by prepared hydrophobic TiO_2 pillared clays was also involved the generation and reaction with $^{\bullet}OH$ radical as in other photocatalytic processes.

Although the photocatalytic activity of prepared photocatalysts modified by CTMAB was slightly lower than that of TiO_2 pillared montmorillonites, this may be play an important role in better understanding of the transfer, transform and photochemical degradation of PAEs onto some natural geoadsorbents in the geochemistry cycle.

Acknowledgements

The authors appreciate the technical assistance from Mrs. Zheng Lin and Mr. Tongshou Xiang. Financial support from the National Nature Science Foundation of China (No. 40302013 and 40572173), Nature Science Foundation of Guangdong Province, China (No. 030466) and the Science and Technology Project of Guangdong Province, China (2005A30401001 and No. 2006A36701002) is also gratefully acknowledged.

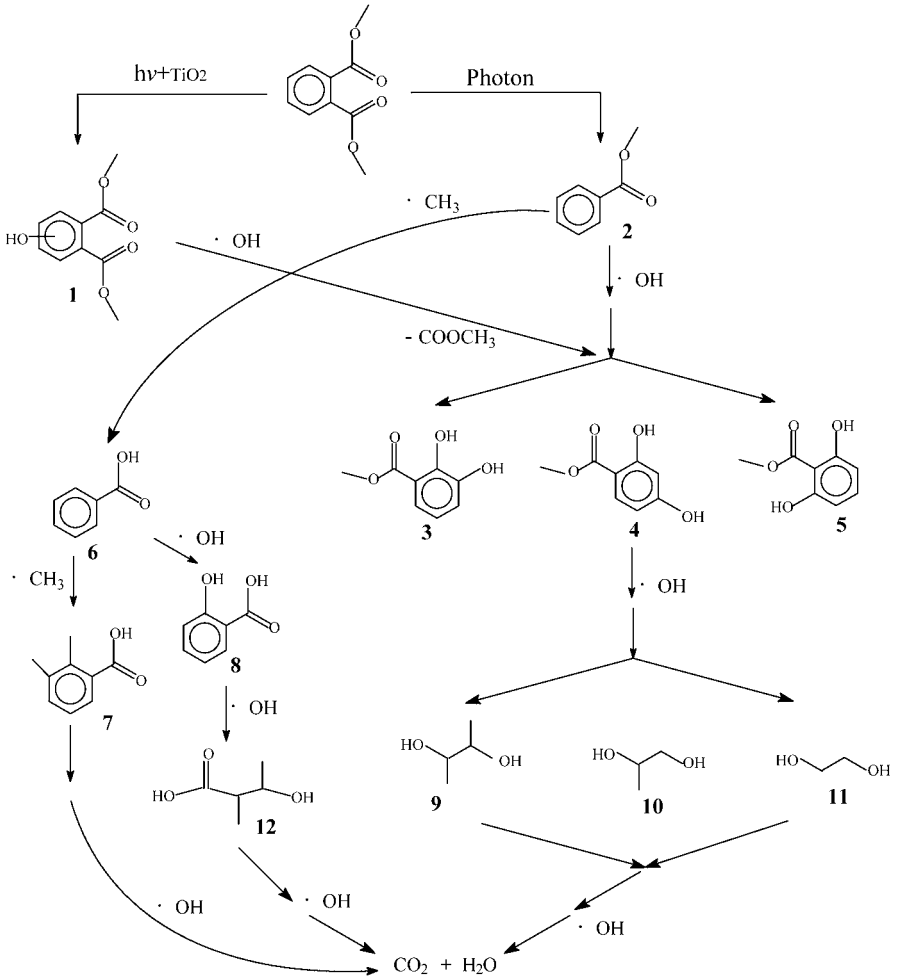

Figure 11. Proposed degradation pathways of DMP in photocatalytic reaction.

REFERENCES

1. M. V. Guidotti and G. M. Cremisini, *Environ. Int.* **23**, 337 (1997).
2. C. A. Staples, D. R. Peterson, T. F. Parkerton and W. J. Adams, *Chemosphere* **35**, 667 (1997).
3. C. S. Giam, H. S. Chan, G. S. Neff and E. L. Atlas, *Science* **199**, 419 (1978).
4. C. Nilsson, in: *Phthalate Acid Esters Used as Plastic Additives, Volume 2: Comparisons of Toxicological Effects*, p. 94. Swedish National Chemicals Inspectorate, Stockholm (1994).
5. W. E. Gledhill, R. G. Kaley, W. J. Adams, O. Hicks, P. R. Michael, V. W. Saeger and G. A. LeBlanc, *Environ. Sci. Technol.* **14**, 301 (1980).
6. C. E. Mackintosh, J. Maldonado, J. Hongwu, N. Hoover, A. Chong, M. G. Ikonomou and F. A. Gobas, *Environ. Sci. Technol.* **38**, 2011 (2004).
7. M. K. Stanley, K. A. Robillard and C. A. Staples, *The Handbook of Environmental Chemistry Part Q. Phthalate Esters*, *Vol. 3*, p. 2. Springer, Berlin (2002).
8. G. R. Douglas, A. P. Hugenholtz and D. H. Blakey, *Environ. Health Persp*. **65**, 255 (1986).
9. L. Keith and W. Telliard, *Environ. Sci. Technol*. **13**, 416 (1979).

10. M. T. Ahmed, A. Dewedar, L. Mekki and A. Dia, *Waste Manage*. **19**, 535 (1999).
11. Y. Wang, Y. Fan and J. D. Gu, *Int. Biodeter. Biodegr*. **53**, 93 (2004).
12. H. Yan and G. Pan, *Chemosphere* **55**, 1281 (2004).
13. G. Alhakimi, L. H. Studnicki and M. Al-Ghazali, *J. Photochem. Photobiol. A: Chem*. **154**, 219 (2003).
14. M. Muneer, J. Theurich and D. Bahnemann, *J. Photochem. Photobiol. A: Chem*. **143**, 213 (2001).
15. A. V. Taborda, M. A. Brusa and M. A. Grela, *Appl. Catal. A: General* **208**, 419 (2001).
16. X. K. Zhao, G. P. Yang, Y. J. Wang and X. C. Gao, *J. Photochem. Photobiol. A: Chem*. **161**, 215 (2004).
17. O. Hocine, M. Boufatit and A. Khouider, *Desalination* **167**, 141 (2004).
18. X. Shen, Y. Lu, S. Wu, J. Sun and L. Zhu, *Chin. J. Environ. Sci.* **25**, 168 (2004).
19. T. Okada, T. Morita and M. Ogawa, *Appl. Clay Sci.* **29**, 45 (2005).
20. D. Yaron-Marcovich, S. Nir and Y. Chen, *Appl. Clay Sci*. **24**, 167 (2004).
21. H. Murayama, K. I. Shimizu, N. Tsukada, A. Shimada, T. Kodama and Y. Kitayama, *Chem. Commun*. **8**, 2678 (2002).
22. R. Swarnakar, K. B. Brandt and R. A. Kydd, *Appl. Catal. A: General* **142**, 61 (1996).
23. C. Ooka, H. Yoshida, M. Horio, K. Suzuki and T. Hattori, *Appl. Catal. B: Environ.* **41**, 313 (2003).
24. C. Ooka, S. Akita, Y. Ohashi, T. Horiuchi, K. Suzuki, S. Komai, H. Yoshida and T. Hattori, *J. Mater. Chem*. **9**, 2943 (1999).
25. Y. Kitayama, T. Kodama, M. Abe, H. Shimotsuma and Y. Matsuda, *J. Poro. Mater*. **5**, 121 (1998).
26. Y. Cai, Z. J. Wang, Y. F. Chen and Z. H. Ge, *Chin. J. Catal*. **19**, 442 (1988).
27. H. Y. Zhu, J. A. Orthman, J. Y. Li, J. C. Zhao, G. J. Churchman and E. F. Vansant, *Chem. Mater.* **14**, 5037 (2002).
28. S. Yamanaka, T. Nishihara, M. Hattori and Y. Suzuki, *Mater. Chem. Phys.* **17**, 87 (1987).
29. C. F. Song, M. K. Lü, P. Yang, D. Xu and D. R. Yuan, *Thin Solid Films* **413**, 155 (2002).
30. P. Qu, J. Zhao, T. Shen and H. Hidaka, *J. Mole. Catal. A: Chem*. **129**, 257 (1998).
31. R. W. Matthews, *J. Catal.* **111**, 264 (1988).
32. S. Turchi and D. Ollis, *J. Catal.* **122**, 178 (1990).
33. O. Bajt, G. Mailhot and M. Bolte, *Appl. Catal. B: Environ*. **33**, 239 (2001).
34. G. Mailhot, M. Sarakha, B. Lavedrine, J. Cáceres and S. Malato, *Chemosphere* **49**, 525 (2002).
35. M. A. Rahman, M. Muneer and D. Bahnemann, *Res. Chem. Intermed*. **29**, 35 (2003).
36. K. Huste and P. N. Moza, *Chemosphere* **17**, 1751 (1988).
37. T. K. Lau, W. Chu and N. Graham, *Chemosphere* **60**, 1045 (2005).
38. A. I. Balabanovich and W. Schnabel, *J. Photochem. Photobiol A: Chem*. **113**, 145 (1988).